Earth Surf. Dynam. Discuss., 3, 1509–1553, 2015
www.earth-surf-dynam-discuss.net/3/1509/2015/
doi:10.5194/esurfd-3-1509-2015

Earth Surface Dynamics Discussions
Open Access
EGU

Coarse bedload routing and dispersion through tributary confluences

K. S. Imhoff and A. C. Wilcox

Department of Geosciences, 32 Campus Drive #1296, University of Montana, Missoula, MT 59812, USA

Received: 31 October 2015 – Accepted: 24 November 2015 – Published: 17 December 2015

Correspondence to: K. S. Imhoff (kurt.imhoff@umontana.edu)

Published by Copernicus Publications on behalf of the European Geosciences Union.

Abstract

Sediment routing fundamentally influences channel morphology and propagation of disturbances. However, the transport and storage of bedload particles in headwater channel confluences, which may be significant nodes of the channel network in terms of sediment routing, morphology, and habitat, is poorly understood. To characterize routing processes through confluences of headwater channels, we investigate how sediment routing patterns through headwater confluences compare to those described in low-gradient gravel bed river systems, and how confluences affect the dispersive behavior of coarse bedload particles compared to non-confluence reaches. We address these questions with a field tracer experiment using passive-integrated transponder and radio-frequency identification technology in the East Fork Bitterroot River basin, Montana, USA. Within the confluence zone, transport occurs along scour hole margins in narrow, efficient transport corridors that mirror those observed in finer-grained experiments and field studies. Coarse particles entering confluences experience reduced depositional probabilities, in contrast to the size-selective transport observed in a control reach. Stochastic transport modeling, tail analysis, and use of a dimensionless impulse (I^*) suggest that transport distance and variance growth are enhanced through confluences for a given flow strength. We suggest that confluences absent of disturbances enhance sediment transport and dispersive growth through headwater networks.

1 Introduction

The spatiotemporal transport and storage patterns of mobile sediment particles through channel networks, i.e., sediment routing (Swanson and Fredriksen, 1982), governs channel evolution in alluvial rivers by linking sediment supply, flow, and channel morphology (Church, 2002, 2006). In headwater regions, where hillslope-channel connectivity is strong and streams are sensitive to spatially and temporally variable forc-

ESURFD
3, 1509–1553, 2015

ing by hillslope processes and land-use change (Montgomery and Buffington, 1997; Brooks and Brierley, 1997; Prosser et al., 2001), debris flows or fluvial processes result in storage and downstream routing of sediment inputs (Lancaster and Casebeer, 2007). Discrete pulses of coarse sediment can travel downstream as a translating bedload wave, as a dispersive process, or as some combination of translation and dispersion (Lisle et al., 2001; Sklar et al., 2009).

Analyses of dispersion based on the premise that particle motion is a random walk have represented downstream transport as a series of intermittent steps and rests (Phillips et al., 2013). This approach has informed flume and field studies seeking to identify characteristic probability distributions of step length and rest period (e.g., Hubbell and Sayre, 1964; Yang and Sayre, 1971; Bradley et al., 2010). Statistical distributions, including exponential, gamma, and Pareto functions, have been found to approximate spatial distributions of bedload particles in flume and field conditions (e.g., Hassan et al., 1991; Bradley and Tucker, 2012; Martin et al., 2012; Haschenburger, 2013). These statistical models have been used to approximate dispersive regimes in various gravel-bed channel morphologies, exploring plane-bed (Bradley and Tucker, 2012), pool-riffle (Liébault et al., 2012; Milan, 2013), and braided systems (Kasprak et al., 2014). Many model functions may be applicable, however, because morphologic features and hydraulics can produce characteristic local dispersive regimes (Pyrce and Ashmore, 2003). Long-term tracer experiments have noted evolving spatial distributions of bedload particles, suggesting that best-fit statistical distributions may differ depending on the degree of vertical mixing, often a function of time (Haschenburger, 2013). As a result, dispersion models predicting a smooth spatial distribution may not adequately capture the true dispersive behavior of bedload particles across multiple channel morphologies. More recent study of coarse bedload transport has considered the dispersive behavior of sediment particles in terms of changes in the variance of particle displacements with time (e.g., Phillips et al., 2013). Sediment dispersion is thus treated as analogous to one-dimensional diffusion in the downstream direction, with potential diffusion dynamics that include normal diffusion, where the variance of

ESURFD
3, 1509–1553, 2015

particle displacements increases linearly with time, and anomalous diffusion, which includes both superdiffusion and subdiffusion, when variance increases more quickly or more slowly with time than the linear case, respectively (Olinde and Johnson, 2015). Predictions of sediment routing require an improved understanding of variability in dispersive regimes among channel types and other controls on sediment dispersion.

Nodes of the channel network that may be especially important with respect to sediment routing are tributary confluences, where point-sources of flow and sediment connect tributary to trunk streams. The importance of confluences in sediment routing, as well as their morphologic significance, may depend on factors including stream densities (i.e., frequency of confluences) (Benda et al., 2004), the magnitude and frequency of disturbances such as debris flows (Benda and Dunne, 1997; Hoffman and Gabet, 2007), and the relative differences in flow, sediment caliber, and load between tributaries and the trunk streams they enter (Fig. 1) (Knighton, 1980; Richards, 1980; Ferguson et al., 2006; Swanson and Meyer, 2014). The morphological effects stemming from disturbance-derived confluence deposits may extend spatially, well beyond the area of flow convergence, and temporally, persisting for $\sim 10^2$–10^4 years (Lancaster and Casebeer, 2007). Study of confluences in light of disturbance deposits and morphological heterogeneity has led to the Network Variance Model (NVM, Benda et al., 2004), which considers the spatial arrangement of confluences in river networks and how they affect local and non-local channel morphological characteristics. Channel confluences also represent biological "hot spots", forcing spatial heterogeneity in habitat types and in various habitat metrics and influencing longitudinal distributions of aquatic organisms (Rice et al., 2001; Gomi et al., 2002).

Whereas sediment dynamics and morphology of headwater confluences can be primarily influenced by disturbances such as debris flows (Benda and Dunne, 1997), what we refer to as "equilibrium" confluence morphology, reflecting feedbacks between flow hydraulics, sediment transport, and morphology, can also develop and persist (Fig. 1). Such confluences, which are well-studied in sand and gravel-bed river systems (e.g., Best, 1987; Rhoads, 1987; Roy and Bergeron, 1990; Biron et al., 1996; Boyer, 2006;

ESURFD
3, 1509–1553, 2015

Rhoads et al., 2009), typically feature a central scour hole, tributary-mouth bars, and bank-attached bars at areas of flow recirculation and stagnation (Best, 1988; Ribeiro et al., 2012). Hydraulics responsible for the formation of this morphology relate to physical controls including junction angle (θ), bed discordance (z_d), discharge ratio (Q_r), and upstream planform curvature (Ashmore and Parker, 1983; Best, 1987; Biron et al., 1996; Rhoads and Sukholodov, 2004; Boyer et al., 2006; Constantinescu et al., 2012; Ribeiro et al., 2012). Sediment transport through equilibrium confluences, however, is poorly understood (Best and Rhoads, 2008), in turn constraining understanding of confluence influences on local and network-scale patterns of sediment routing.

In this study we assess how coarse bedload particles are routed through equilibrium confluences in a mountain river headwaters. We address two questions: (i) How do sediment routing patterns through headwater confluences compare to those described in other, primarily lower-gradient gravel-bed river systems? (ii) How do confluences affect the dispersive behavior of coarse bedload particles compared to non-confluence reaches? We address these questions with a tracer experiment, using passive-integrated transponder (PIT) tags, conducted through two headwater confluences and a non-confluence control reach. We employ established sediment transport models, tracer analyses, and a dimensionless impulse framework (Phillips et al., 2013) to explore the effects of confluences on sediment transport and dispersive behavior. Lastly, we compare our results and their implications with theory regarding confluences and sediment routing through headwater networks. Our study contributes to the growing body of work on particle dispersion and transport dynamics in mountain rivers and is, to our knowledge, the first to investigate these topics with respect to sediment routing through confluences in a field setting.

ESURFD
3, 1509–1553, 2015

2 Methods

2.1 Study area

We selected a study area in the East Fork Bitterroot (EFB) River basin in western Montana, USA (Fig. 2) that is typical of semiarid, snowmelt-dominated, montane headwater systems lacking recent disturbance and containing confluences exhibiting characteristics of the equilibrium morphology described above. The field site drains 298 km^2 of forested and alpine mountainous terrain, in both the Sapphire Mountains and Pintler Range, ranging in elevation from 1584 to 2895 m. Sediment supplied to channels is comprised of quartzite, argillite, siltite, and feldspathic granitic rock, eroded from metasedimentary Belt Supergroup and Idaho Batholith sources. Annual precipitation is about 0.6 $m\,yr^{-1}$, based on data from the Tepee Point weather station 1.4 km from the EFB (Western Regional Climate Center Remote Automated Weather Station, 2015). Runoff is dominated by spring snowmelt, with flows capable of mobilizing coarse bedload typically occurring in similar streams between March and July. Human influences from roads and other land uses are minimal in the study area.

Two tributary confluences mark the upstream and downstream extent of the study area. These are herein referred to as the upper confluence, where Moose Creek and Martin Creek combine, and, 1 km downstream, the lower confluence, where Martin Creek enters the EFB. The tributary and mainstem stream of each study confluence are considered as separate reaches, for the purpose of separately considering incipient motion and transport behavior of tracers starting in each. Between the study confluences is a plane-bed-morphology control reach. Combined discharge in the upper confluence is approximately half that of the lower confluence. Depositional bars are present behind large flow obstructions such as logs or large boulders, and along channel margins. Because the site is ungauged, we installed HOBO-U20 water level loggers to record stage at 15 min intervals during the 2014 study period. One transducer was placed along a surveyed-cross section of the bed at each study reach. We also periodically manually measured water surface elevations and, dur-

ESURFD
3, 1509–1553, 2015

ing wadeable conditions, stream velocities. Above-average flows during the study period reflected that year's large snowpack. Snow water equivalent at SNOTEL sites within 50 km of the study area registered above 150 % of normal on 1 April 2014 (http://www.wcc.nrcs.usda.gov/snow/).

To characterize study-reach morphology, we completed topographic surveys and grain-size measurements. Topography was surveyed using a Leica TS06 total station during the initial tracer deployment (March 2014), before spring runoff high flows, and the summer (July–September) recovery campaign. Topographic surveys entailed longitudinal profiles, to determine slope, and cross-sections at the location of pressure transducers, for use in the incipient motion estimates described below. We also surveyed bedform extents to produce a bedform map. Surface grain size distributions were measured using Wolman pebble counts across each study reach. Channel slopes, dimensions, grain sizes, and confluence characteristics are shown in Table 1 (also see Supplement).

2.2 Tracer preparation, deployment, and measurement

Our study employed passive-integrated transponder (PIT) and radio-frequency identification (RFID) technology for tagging and tracing particles. PIT tags are highly recoverable, durable, and cost-effective relative to other particle tracing methods (e.g., Lamarre et al., 2005; Bradley and Tucker, 2012; Chapuis et al., 2015). Moreover, PIT-tagging allows for analyses of transport of both bed-material populations and specific subsets of the grain population (e.g., by size, shape, lithology), step-length distributions and their evolution over time, and other aspects of transport dynamics.

We collected gravel and cobble particles from Moose Creek, upstream of our study reaches, in January 2014 for tagging. Using a 1 hp drill press, holes 8 mm wide by 30 mm long were drilled using a ~ 0.8 mm diamond-tipped drill bit. Tracer particles used were larger than the bed D_{50}, as particles with b axis below 45 mm often fractured during drilling. We tagged cobbles with median axes mostly between 60 and 130 mm (Fig. 3). This represents the D_{37} to D_{70} size fraction, which we assumed to

ESURFD
3, 1509–1553, 2015

be representative of the coarser fraction of mobile bedload particles. The results and interpretation of our sediment tracers thus do not apply for the entire mobile bedload population in this system.

The passive-integrated transponder (PIT) tags used in this study are 12 and 23 mm half-duplex, read-only tags. Each tag is comprised of a glass-encapsulated pulse transponder that emits a unique identification code when activated (Lamarre et al., 2008). By deploying a reading unit and control unit, an electromagnetic signal can be emitted that briefly powers the passive transponder, which then transmits its unique identification code. Inserted PIT tags were sealed in tracer particles with marine epoxy. The tags were activated and the identity and size of each rock recorded prior to deployment. Liébault et al. (2012) found post-drilling density differences to be small (3–5 %), so we did not consider the density differences post-implantation in this study. In total, 428 cobble and gravel tracers were prepared for deposition into the three study reaches; these were distributed among sites as shown in Table 2.

We installed the PIT-tagged tracers before the onset of the spring snowmelt, in late March and early April 2014. Our seeding method emulated that employed by Ferguson and Wathen (1998): particles were seeded loosely on the bed surface near the channel thalweg in a random grid, so the tracers were most likely to move to natural positions from which further dispersion could be monitored. Additionally, a sparse grid helps avoid disturbance to the bed and flow field (Bradley and Tucker, 2012) while simultaneously avoiding "confusing" the PIT tag detection equipment, which encounters issues when dealing with clusters of particles (Chapuis et al., 2014). The gridded surface ranged from 7–13 m wide. We deployed PIT-tagged tracers at equal distances upstream from the confluence in each tributary. Initial tracer positions were recorded using the total station.

Field recovery campaigns to detect tracer locations and measure particle displacement took place after recession of high flows, once the streams were wadeable. This entailed scanning the bed with a 0.5 m diameter loop antenna, in conjunction with a backpack reader. Once a tracer was located, the loop antenna was brought towards

ESURFD
3, 1509–1553, 2015

its detection field from all directions. This helped to identify other tracers in a cluster by reading different tags first, depending on the direction the cluster is approached. Each tracer's position was recorded using the total station. We also employed a snorkel survey to identify if tracers were exposed on the bed or clustered together. Visible tracers were occasionally surrounded by other tracers in shallow pockets. At all sites, we scanned with the loop antenna for 200 m downstream of the last detected particle to limit omission of any far-traveling tracers, which influence the tail character of step-length distributions. The position of far-traveling tracers was recorded with a Trimble GEOXH 6000 GPS.

Both the total station and loop antenna introduce error in measurements of tracer position and travel distance. Individual measurements for the Leica total station have an inherent uncertainty of ±0.20 m. The detection range for the loop antenna differs based on the orientation of the PIT tag relative to that of the loop. Lamarre et al. (2005) identified horizontal and vertical detection ranges at 0.35 and 0.5 m, respectively, and Bradley and Tucker (2012) record a vertical range of 0.25 m. An in-depth assessment of RFID detection ranges is presented by Chapuis et al. (2014), and identifies higher uncertainty in radial detection distance than reported in other studies. The most uncertain tracer position is that of a solitary, buried tracer, which is not visible via snorkel survey and has the largest detection radius – clusters of buried tracers have reduced detection ranges via tag interference. We oriented the antenna parallel to the surface of the bed, at a height of about 0.2 m (after Chapuis et al., 2014). For our analysis, we considered tracers moving greater than 0.2 m as the "mobile" fraction; tracers measured as moving 0.2 m or less were considered immobile and assigned a travel distance of 0 m.

2.3 Transport analyses

We conducted a suite of analyses to evaluate how particle displacement through the study confluences compared to that of the control reach. We assessed stochastic sediment transport models of sediment dispersion across our study site, scaled tracer transport and tail character, and a dimensionless impulse, with the goal of evaluating

ESURFD
3, 1509–1553, 2015

and comparing dispersive regimes. Additional details on these analyses, beyond what is provided below, are in Supplement and Imhoff (2015).

2.3.1 Stochastic sediment transport modelling

To determine whether step-length distributions in confluence reaches differ from those in the control reach, we tested the applicability of two models of sediment dispersion: the Einstein–Hubbel–Sayre (EHS; Hubbel and Sayre, 1964) and Gamma-Exponential models (GEM; Yang and Sayre, 1971). These models were chosen because the EHS and GEM functions have been used to fit step-length probability distributions for a similar plane-bed reach in Colorado (Halfmoon Creek; Bradley and Tucker, 2012); our tracer seeding methods were similar to that study. The primary difference between the EHS and GEM models is whether or not the distribution of step lengths monotonically decreases (EHS) or not (GEM), through the use of exponential and gamma distributions for step length, respectively. Comprehensive background on the use of these models is provided by Bradley and Tucker (2012). We compared EHS and GEM fits to our confluence and non-confluence transport data, with the goal of comparing bulk routing characteristics between the two reach types.

2.3.2 Modal transport and tail analysis

To determine dimensionless transport distances of each tracer, i.e., modal transport distance, we scaled each tracer's transport distance (X_i) by its median diameter (D_i). We then calculated normalized transport distance, X_n (after Phillips et al., 2013):

$$X_n = \frac{\frac{X_i}{D_i}}{\left\langle \frac{X}{D} \right\rangle} \quad (1)$$

where ($\langle X/D \rangle$) is the mean step length for the 2014 flood at each study reach. Relative tracer transport distances and group statistics can thus be compared among populations of mobile particles. We also investigated size-selective transport by plotting scaled

ESURFD
3, 1509–1553, 2015

travel distance ($L^* = L_i/L_{50}$) against scaled tracer size ($D^* = D_x/D_{50}$) for 10 mm subsets of our tracers, where L_i is the mean travel distance of each subset, L_{50} the mean travel distance for the entire population, D_x the mean value of each subset, and D_{50} the median grain size of the bed. We also assessed how our transport distance-grain size relationship compared to the empirical, size-dependent transport relationship for gravel-bed rivers developed by Church and Hassan (1992):

$$\log L^* = 0.232 + 1.35 \log(1 - \log D^*), \quad (2)$$

a relationship that suggests that, as scaled particle size increases, scaled travel distance decreases.

A second method for assessing the evolution of sediment pulses in right-skewed statistical distributions is to analyze tail character of a tracer population (Hassan et al., 2013). Heavy-tailed step-length distributions occur when a large proportion of particles travel relatively long distances. We analyzed cumulative exceedance distributions of tracer travel distance for each study reach to assess tail character. This was achieved by measuring the rate of decay of the exceedance distribution tail, $P(X > x)$, where X is a travel distance beyond the user-determined start of the tail, x, and heavy tailedness is defined as when the log-log slope of decay (α) is less than 2 (after Hassan et al., 2013). The mean and variance of step-length distributions converge to finite values in thin-tailed cases ($\alpha > 2$); the mean is finite but variance non-convergent when $1 < \alpha < 2$; neither mean nor variance converge to finite values when $\alpha < 1$ (Olinde and Johnson, 2015).

2.3.3 Incipient motion and dimensionless impulse

We also analyzed tracer data with respect to a cumulative dimensionless impulse, I^* (Eq. 3), determined for each of our five seed reaches. I^* allows for a fluid momentum conservation approach to analyze long-term tracer displacement data and was developed to allow for pairing such data with simple flow and bed measurements. We

ESURFD
3, 1509–1553, 2015

used I^* to compare tracer transport distances against the cumulative excess shear stress imparted on grains. When comparing confluence and non-confluence reaches, we considered deviation from a linear relationship between $\langle X/D \rangle$ and I^* (Phillips et al., 2013) to constitute a difference in dispersive regimes. The impulse, I^*, is defined as follows:

$$I^* = \int_{t_i}^{t_f} \frac{(U_e^*)\mathrm{d}t}{D_{50}} \tag{3}$$

where t_i and t_f are start and end times, respectively, for flow above a critical threshold of motion of bed materials, and U_e^* is excess shear velocity, which is the difference between the shear velocity (U^*) and the critical shear velocity (U_c^*) associated with initial motion of bed particles. Flume studies have identified that a mobilized sediment particle shows a step length that is proportional to U_e^* (Lajeunesse et al., 2010; Martin et al., 2012). Shear velocity is equal to $(gRS)^{0.5}$ where g is gravitational acceleration, R is hydraulic radius, and S is channel slope; for the critical condition (U_c^*), R_c is critical hydraulic radius associated with the mobilization of the average-sized tracer particle. We back-calculated R_c from critical Shields number (τ_c^*), a non-dimensional shear stress associated with incipient motion of particles in a flow:

$$\tau_c^* = \frac{\rho g R_c S}{((\rho_s - \rho_w) g D_{50})} \tag{4}$$

where ρ_s is sediment bulk density (assumed to equal 2650 $\mathrm{kg\,m^{-3}}$) and ρ_w is water density (1000 $\mathrm{kg\,m^{-3}}$).

Because our tracer equipment could not directly detect the conditions under which particles were mobilized, we instead estimated a range of τ_c^* using two equations derived from similar gravel-bed systems. For the first estimate, we used Mueller et al.'s (2005) reference dimensionless shear stress relation for steep gravel and cobble-bed

ESURFD
3, 1509–1553, 2015

rivers:

$$\tau^*_{c,\,\text{Mueller}} \approx \tau^*_r = 2.18S + 0.021 \quad (5)$$

where τ^*_r is a reference shear stress, which we assume is similar to τ^*_c (after Mueller et al., 2005). The river in Mueller et al.'s study, Halfmoon Creek, is similar to our study site with respect to channel dimensions, critical discharge, hydrology, elevation, and bed sediment characteristics. For a second estimate of τ^*_c, we used Recking's (2013) mobility shear stress (τ^*_m) equation, which was empirically developed using bedload transport data from gravel-bed transport studies in mountainous streams:

$$\tau^*_{c,\,\text{Recking}} \approx \tau^*_m = (5S + 0.06)\left(\frac{D_{84}}{D_{50}}\right)^{4.4\sqrt{S}-1.5} \quad (6)$$

where D_{84} is the 84th percentile grain size. As with Eq. (5), we assume τ^*_m approximates τ^*_c (after Recking, 2013).

These two estimates for τ^*_c were paired with stage data to estimate the cumulative duration of flow above the threshold of motion, a value that varies in time and space and is therefore difficult to measure directly (Charru et al., 2004). At each seed reach, we identified the depth at each reach's pressure transducer (h_c) that pairs with the R_c for initiating sediment motion, thus linking stage data to estimates of channel-averaged U^* during the 2014 flood hydrograph. Estimates of U^*_e were then integrated across the 2014 hydrograph to estimate I^*. Because Eq. (3) is restricted only to flow above the threshold of sediment motion, I^* limits the frequency-magnitude distribution of U^* to conditions relevant to estimated sediment transport and only considers the momentum excess imparted by the flow on sediment particles. This approach adopts the simplifying assumption of a constant U^*_c for a given field site (after Phillips et al., 2013), although we recognize that U^*_c likely varies in both space and time.

ESURFD
3, 1509–1553, 2015

3 Results

3.1 2014 flood hydrology

Flow stage at all transducer locations rose sharply around 1 May, peaking between 25 May and 4 June, depending on the reach (Supplement). The 2014 flood hydrograph at the East Fork Bitterroot seed reach, lower confluence, is shown in Fig. 4. Flow stage at different sites exceeded the estimated threshold of incipient motion for 8–37 ($\tau^*_{c,\,\mathrm{Mueller}}$) or 1–17 ($\tau^*_{c,\,\mathrm{Recking}}$) days, with the lower confluence experiencing the longest duration above the critical level. We used the transducer data, along with Parrett and Johnson (2004) and analysis of a downstream US Geological Survey gauge, to estimate the peak discharge in 2014 as a 3.5 to 4 year event.

3.2 Tracer recovery and displacement

We recovered of 75 % of the seeded tracers. Recovery was greatest within study reaches with low D_{84} values and short transport distances, including the control reach and Moose Creek (Table 2). Our recovery rate is comparable to recent tracer studies using RFID technology: 25–78 % (Liébault et al., 2012), 93–98 % (Bradley and Tucker, 2012), 62–100 % (Phillips et al., 2013), 40 % (Chapuis et al., 2015).

Similar percentages of recovered tracers (41, 39, and 50 %) left each seed reach. At the upper confluence, tracer configurations within the seed reach retained their gridded spatial pattern in Moose Creek but not in Martin Creek, which contained more boulders to facilitate trapping and clustering of particle tracers (Fig. 5). Particles seeded in Moose Creek also constituted the majority of tracers exported into the confluence itself. Deposition within the confluence primarily correlated to depositional bars flanking the scour hole (Fig. 6). Particles deposited within the scour hole were segregated by contributing stream. No tracers from the upper confluence were recovered beyond the extent of the equilibrium confluence morphology in the upper confluence.

ESURFD
3, 1509–1553, 2015

Particles recovered in the lower confluence largely retained the gridded arrangement of their initial positioning at both seed reaches. The relative contribution of tracers into the confluence was more evenly distributed than in the upper confluence: 55 % of deposited tracers came from the East Fork, with the remaining 45 % from Martin Creek. Similar to the upper confluence, tracer particles remained segregated as they progressed through the confluence, stranding preferentially on bank-attached depositional bars. Deposition within the scour hole was limited and segregated, further agreeing with the upper confluence. An additional group of tracers, seeded at the upstream junction corner, were immobile. Similar to the upper confluence, large boulders were effective in trapping mobile tracer particles. Of the recovered tracers in the entire lower confluence, 23 % left the confluence zone completely, with 58 % of post-confluence tracers originating in the East Fork and 42 % from Martin Creek. Recovered particles downstream of the lower confluence cease to be segregated after about 30 m, and were recovered approximately in the channel center.

3.3 Model results

The Einstein–Hubbell Sayre (EHS) and Yang–Sayre (GEM) models provided similar-quality fits to each other in all study reaches. The Yang–Sayre GEM provides the most accurate fit, with a slight R^2 advantage ranging from 0.01 to 0.001. Both the EHS and GEM models deliver accurate approximations of the slowest-moving tracer bins before generally overestimating the probabilities of mid-range bins and underestimating the probabilities of fast-moving bins. Fast-moving tracer bins underpredicted by the models correspond to the tail of the step-length probability distribution. In the control reach, fast tracer bins generally have a smaller residual than in the confluence study reaches (Fig. 7). The models fit the lower confluence tracers better than the upper confluence tracers (Table 3). In all reaches but Martin Creek (lower confluence), the average transport distance of our data exceeded model estimates (Table 3).

ESURFD
3, 1509–1553, 2015

3.4 Effects on travel distance

3.4.1 Tracer dispersion

At the upper confluence, mobile tracers entering the confluence zone exhibited a distinct step in the spatial distribution of tracer positions, denoting enhanced transport and reduced depositional probabilities (Fig. 8, after Haschenburger, 2013). Enhanced transport is also evident for tracers routing through the lower confluence reaches (Fig. 8): a distinct step is evident for tracers entering the confluence, where the probability of deposition decreases for the duration of time spent within the confluence zone. Compared to the confluence reaches, the control reach lacks significant steps and instead features a smooth decay.

Dimensionless step-length distributions deviate from a best-fit exponential distribution at distances beyond approximately twice the average normalized transport distance (Fig. 9). In evaluating X_n, tracers in the upper confluence reaches do not travel as far relative to the population mean as those in other seed reaches. When we assessed tail character, confluence populations generally showed smaller α values than the control reach, corresponding to heavier tails and greater dispersive growth. However, the point of origin of the tail is user-defined, and varying the start point changes the resulting slope of the exceedance tail. We therefore assessed tail character at multiple points above the 75th percentile, to test the sensitivity of tail designation (thin or heavy). None of the study reaches cross the thin-heavy threshold by varying the tail start point, though α values are sensitive. We settle for defining the tail as beginning at the 80th percentile (Fig. 10). Only Moose Creek shows a thinner tail in the exceedance probability distribution than the control. Martin Creek (at both the upper and lower confluences) exhibits a heavy-tail, while Moose Creek, the control, and East Fork Bitterroot are thin-tailed.

ESURFD
3, 1509–1553, 2015

3.4.2 Grain size and travel distance

Figure 11 shows our tracer transport data, among 10 mm subsets from 60 to 130 mm particles, compared to Church and Hassan's empirical relationship for size-dependent transport (Eq. 2). The control reach tracers largely agreed with size-selective transport characteristics, with the largest residual relative to the curve occurring for the largest grain-size bins, which experienced shorter transport distances than what would be expected from Eq. (2). The two confluence sites showed worse agreement to the empirical curve of Church and Hassan (1992). The upper confluence shows nearly equal transport distances across all grain-size bins, while the lower confluence data show a peak in mobility for particle sizes around the tracer median.

3.4.3 Dimensionless impulse

Our estimates of critical Shields number ranged from 0.056 to 0.109 (Table 4). For all study reaches, $\tau^*_{c,\,\mathrm{Mueller}}$ values (Eq. 5) were lower than the $\tau^*_{c,\,\mathrm{Recking}}$ values (Eq. 6), predicting correspondingly lower U^*_c values. The distribution of U^* scales with channel dimensions and peak discharge, with the upstream confluence seed reaches experiencing smaller U^* values than the control reach and lower confluence. As I^* depends on the estimated threshold of motion for each study reach, itself a function of grain size and hydraulic radius, we note a reliance of I^* on channel roughness. The difference between I^* estimates also varies as a function of hydraulic radius. Moose Creek, for example, is wider and shallower than Martin Creek at the upper confluence, and requires a larger discharge increase to move from the Mueller to Recking incipient motion threshold estimate. This results in reach-specific variation in sensitivity to the estimation method for incipient motion.

We found $\langle X/D \rangle$ to conform to a linear relation to I^*, and variance (σ^2) to a power-law function, in agreement to the predictions and findings of Lajeunesse et al. (2010), Phillips et al. (2013), and Phillips and Jerolmack (2014) (Fig. 12). Fits could be greatly improved when only considering the relationship between confluence reaches: the con-

ESURFD
3, 1509–1553, 2015

trol reach has similar displacement but higher l^* values than reaches at the upper confluence, giving it the highest residual from the best-fit curve in both cases.

4 Discussion

4.1 Coarse-sediment routing through confluences

Our study used PIT/RFID technology to provide novel insights into the effect of tributary confluences on sediment routing through mountain streams. Maximum transport distances along scour-hole flanks and segregation are similar to the findings of Mosley (1976) and Best (1988). Because we detect no tracers beyond the extent of the upper confluence, we take the depositional pattern in Fig. 6 to reflect a tendency of our tracers to route along, rather than through, the scour hole. We do not know how tracers recovered beyond the lower confluence progressed through the confluence itself, but we see similar depositional patterns and posit that similar transport corridors apply. We consider these transport patterns to reflect the controlling influences of θ and Q_r; the simple upstream planform geometry and minimal bed discordance at our sites suggest that these factors have less influence on confluence morphodynamics. Observed discordance between scour and tributary mouth bars at our study confluences (0.6 and 1.4 m, respectively) exceed that of Roy and Bergeron (1990; ~ 0 m at $\theta = 15$), supporting observations that scour is largely absent at low θ values (Benda and Cundy, 1990).

Our data also agree with the assertions of Best (1988) and others as to how the position and orientation of the scour hole is influenced by Q_r. Increased penetration of flow from the tributary at the upper confluence, due to higher Q_r, forced the scour hole towards the middle of the confluence, as opposed to the lower confluence where the scour was shifted by greater discharge from the East Fork Bitterroot. Observed feedbacks between confluence morphology and particle transport suggest similar confluence morphodynamics as observed in past studies (e.g., Mosley, 1976; Best, 1987;

ESURFD
3, 1509–1553, 2015

Boyer et al., 2006; Rhoads et al., 2009), though in a higher-gradient, more headwaters setting than previous work.

4.2 Effects of confluences on dispersion

Fit quality of the EHS and GEM models support Bradley and Tucker's (2012) assertion that a gamma or exponential distribution can approximate the true compound Poisson distribution of step lengths in a plane-bed morphology. The monotonically decreasing nature of the EHS is responsible for inferior fits relative to the GEM, similar to the observations of Bradley and Tucker (2012), though differences between the two at our site are almost indistinguishable. We can only assume the EHS and GEM to provide adequate fits over short time periods, as our work and that of Bradley and Tucker (2012) cover 1–4 flood events. In our case the majority of recovered tracers were not vertically mixed, and fits are likely to weaken over time as particles become vertically integrated with the bed (Haschenburger, 2013). Quality of fit was generally similar between confluence and non-confluence reaches, except for fast-moving tracers in the tail, in which confluence reaches deviated more from model data. This suggests that the two types of reaches differ, although not sufficiently to cause highly inaccurate model fits at the scale of individual floods and confluences.

The steps we observe in spatial distributions of our tracers (Fig. 8) suggest adjusted depositional rates with distance through confluences. Coarse sediment tracers moving through the confluence zone are less likely to deposit within the confluence relative to the seed reach preceding it. This is further suggested by the comparative travel distances of different-sized particles through our study confluences. We see the weakest relationship between grain size and travel distance for tracers in the upper confluence seed reaches, where the largest proportion of bed distance occurs within the confluence zone (Fig. 11). In the control reach, size-selective transport emerges in contrast to the tracer populations moving through confluences. We assert that coarse particles entering confluence zones are less likely to deposit than in the preceding channel reach, especially for larger grains. Enhanced transport is further suggested by nor-

ESURFD
3, 1509–1553, 2015

malized transport distance (X_n) and heavier tails (Figs. 9 and 10), where a greater proportion of tracers in confluence reaches move relatively longer distances compared to reach-specific average transport. By capturing one flood event, we were unable to conduct analyses concerning the scaling of time to dispersive growth or comment on the nature of diffusion, as done by Olinde and Johnson (2015) and others. Despite this, observed tracer transport suggests that confluences enact an enhanced dispersive regime through increased travel distances and reduced depositional probabilities.

4.3 Confluences and large-scale sediment routing

We propose a conceptual model where equilibrium confluences have the effect of enhancing coarse bedload transport and dispersion downstream. While model fits were not greatly different between control and confluence reaches, we expect this effect to increase in significance as coarse particles are routed through multiple confluences. This model applies to confluence morphology that is governed by hydraulics and sediment supply typical of snowmelt-dominated hydrographs, as opposed to confluences influenced by recent disturbance. We consider our model within the context of Benda et al.'s (2004) Network Variance Model, to consider the effects of confluences at the scale of headwater river networks. The NVM considers that the likelihood of morphologically significant perturbations to mainstem channels, in the form of large sediment deposits, increases in the vicinity of confluences due to upstream disturbance. Our sites, where recent tributary disturbances are absent, diverge from this model, such that sediment can propagate, unhindered by past sediment deposits, through confluence zones, and indeed, transport is enhanced rather than impeded across our equilibrium confluences. Our work expands, rather than refutes, the NVM by suggesting that confluences play morphologically important roles with respect to sediment routing both in and outside of disturbance-dominated headwater systems.

We hypothesize, based on our findings above, that sediment routing through individual equilibrium confluences influences routing at the larger basin scale in mountain watersheds. As the equilibrium confluence is contingent on high Q_r, θ, and other phys-

ESURFD
3, 1509–1553, 2015

ical controls, we would expect certain basin types to accumulate confluence effects to a greater extent than others, according to basin shape, drainage density, and network geometry (Benda et al., 2004). As an illustrative example, we compare the EFB basin to a similarly sized basin (Tin Cup Creek) in the nearby Bitterroot Range (Fig. 13). The morphology of basins in the Bitterroot vs. Sapphire Mountains differ considerably as a result of differences in erosive history and lithology. The Bitterroot are formerly glaciated and have granitic rock, with U-shaped valleys, elongate basins, and trellis networks. The unglaciated Sapphires, in contrast, have V-shaped valleys, compact basins, and dendritic networks. Comparing these basin types, basins such as those in the Sapphire Range (e.g., the upper EFB basin) have larger tributary channels of increasing order (Strahler, 1952), where tributary discharges scale with increased mainstem flow, and a greater number and downstream extent of equilibrium confluences than elongate basins (Benda et al., 2004) like those in the Bitterroot. Other basin factors, such as network geometry and distance between equilibrium confluences, are further expected to govern confluence effects on nonlocal sediment routing (Benda et al., 2004). This suggests that basin shape, itself a function of lithology and climate, may provide information regarding dispersive behavior of a coarse bedload population, determining the setting where confluences would be expected to enact a cumulative and significant effect on coarse sediment transport.

Understanding the extent to which equilibrium confluences affect basin-scale routing requires further insight into coarse bedload connectivity in mountain rivers. Our conceptual model assumes steady progression of coarse sediment downstream in a plane-bed morphology; however, discontinuity in coarse sediment transfer can emerge when competence is reduced and particles enter long-term storage (e.g., Tooth et al., 2002; Hooke, 2003; Fryirs, 2013; Bracken et al., 2015). Certain channel morphologies exhibit bedload particle displacements between morphologic units (e.g., bars; Pyrce and Ashmore, 2003), which can result in disconnectivity if bedform-scale aggradation exceeds rates of removal (Hooke, 2003). Ultimately, the unique dispersive patterns we observe at the scale of individual confluences must be analyzed cumulatively, across

ESURFD
3, 1509–1553, 2015

multiple confluences and within other channel morphologies, to quantify the extent of their influence over large-scale patterns of sediment routing.

5 Conclusions

Our study, the first to date of coarse-sediment routing through mountain-river confluences, showed that in gravel-bed headwater systems, tributary confluences represent geomorphically unique locations that locally affect patterns of sediment routing. At the reach scale, coarse sediment is routed through confluences along the flanks of a well-defined scour hole, in agreement with observations and flume studies from other gravel-bed systems. Transport distance of mobilized clasts through the confluence zone is less dependent on grain size than in the plane-bed channel morphology, especially for larger grains. We found confluence reaches to impart greater transport distances and dispersive growth compared to the plane-bed channel morphology, even when particles did not progress beyond the downstream extent of the confluence itself. Our study also illustrates the utility of tracer studies using PIT/RFID technology for providing field-based insights into sediment transport dynamics.

We proposed a conceptual model where equilibrium headwater confluences promote enhanced dispersion and greater downstream transport distances than otherwise expected. According to the sediment cascade framework of Fryirs (2013), this would classify equilibrium confluences as an enhanced longitudinal linkage compared to the plane-bed channel morphology. The conceptual model posited herein adds to previous study by suggesting that sediment routing through fluvially dominated confluences alters overall particle dispersion. Combined with the work of Benda et al. (2004) and others, we suggest that the location of confluences influences sediment routing patterns and, in the case of upstream disturbances, responses to sediment pulses, in headwater systems both with and without disturbance-derived sediment deposits. These results pertain to a range of problems in headwater networks, including solid-phase contaminant transport (Bradley et al., 2010), cosmogenic radionuclide accumulation

ESURFD
3, 1509–1553, 2015

(Gayer et al., 2008), sediment budgeting (Malmon et al., 2005), and the duration and topographic impact of pulses on aquatic habitat (Lisle et al., 2001).

The Supplement related to this article is available online at doi:10.5194/-15-1509-2015-supplement.

Acknowledgements. We thank P. A. Duvillard, A. Maphis, D. Davis, M. Jahnke, and A. Sawyer for exceptional assistance during the 2014 field season. We thank M. Hassan, L. Eby, M. Maneta, S. Bywater-Reyes, and R. Manners for valuable insight in the planning and implementation of this work. We thank N. Bradley and C. Legleiter for aid in model use and coordinate transformation. We thank C. Phillips for assistance in performing impulse analyses. This work was supported by the Montana Institute on Ecosystems' award from the National Science Foundation EPSCoR Track-1 program under Grant # EPS-1 101 342. This work was also supported by grants from the Montana Geological Society, the Geological Society of America, and the Northwest Scientific Association.

References

Ashmore, P. and Parker, G.: Confluence scour in coarse braided streams, Water Resour. Res., 19, 392–402, 1983.

Benda, L. and Cundy, W.: Predicting deposition of debris flows in mountain channels, Can. Geotech. J., 27, 409–417, 1990.

Benda, L. and Dunne, T.: Stochastic forcing of sediment routing and storage in channel networks, Water Resour. Res., 33, 2865–2880, 1997.

Benda, L., Andras, K., Miller, D., and Bigelow, P.: Confluence effects in rivers: interactions of basin scale, network geometry, and disturbance regimes, Water Resour. Res., 40, W05402, doi:10.1029/2003WR002583, 2004.

Best, J.: Flow dynamics at river channel confluences: implications for sediment transport and bed morphology, Soc. Econ. Pa., 39, 27–35, 1987.

Best, J.: Sediment transport and bed morphology at river channel confluences, Sedimentology, 35, 481–498, 1988.

ESURFD
3, 1509–1553, 2015

Best, J. L. and Rhoads, B. L.: Sediment transport, bed morphology and the sedimentology of river channel confluences, in: River Confluences, Tributaries and the Fluvial Network, JohnWiley and Sons, Chichester, UK, 45–72, 2008.

Biron, P., Best, J. L., and Roy, A. G.: Effects of bed discordance on flow dynamics at open channel confluences, J. Hydraul. Eng.-ASCE, 122, 676–682, 1996.

Boyer, C., Roy, A. G., and Best, J.: Dynamics of a river channel confluence with discordant beds: flow turbulence, bed load sediment transport, and bed morphology, J. Geophys. Res., 111, F04007, doi:10.1029/2005JF000458, 2006.

Bracken, L. J., Turnbull, L., Wainwright, J., and Bogaart, P.: Sediment connectivity: a framework for understanding sediment transfer at multiple scales, Earth Surf. Proc. Land., 40, 177–188, doi:10.1002/esp.3635, 2015.

Bradley, N. and Tucker, G. E.: Measuring gravel transport and dispersion in a mountain river using passive radio tracers, Earth Surf. Proc. Land., 37, 1034–1045, doi:10.1002/esp.3223, 2012.

Bradley, D. N., Tucker, G. E., and Benson, D. A.: Fractional dispersion in a sand bed river. J. Geophys. Res., 115, F00A09, doi:10.1029/2009JF001268, 2010.

Brooks, A. and Brierley, G.: Geomorphic responses of lower Bega River to catchment disturbance, 1851–1926, Geomorphology, 18, 291–304, 1997.

Chapuis, M., Bright, C. J., Hufnagel, J., and MacVicar, B.: Detection ranges and uncertainty of passive Radio Frequency Identification (RFID) transponders for sediment tracking in gravel rivers and coastal environments, Earth Surf. Proc. Land., 39, 2109–2120, doi:10.1002/esp.3620, 2014.

Chapuis, M., Dufour, S., Provansal, M., Couvert, B., and de Linares, M.: 2015, coupling channel evolution monitoring and RFID tracking in a large, wandering, gravel-bed river: insights into sediment routing on geomorphic continuity through a riffle–pool sequence, Geomorphology, 231, 258–269, doi:10.1016/j.geomorph.2014.12.013, 2015.

Charru, F., Mouilleron, H., and Eiff, O.: Erosion and deposition of particles on a bed sheared by a viscous flow, J. Fluid Mech., 519, 55–80, doi:10.1017/S0022112004001028, 2004.

Church, M.: Geomorphic thresholds in riverine landscapes, Freshw. Biol., 47, 541–557, doi:10.1046/j.1365-2427.2002.00919.x, 2002.

Church, M.: Bed material transport and the morphology of alluvial river channels, Annu. Rev. Earth Pl. Sc., 34, 325–354, doi:10.1146/annurev.earth.33.092203.122721, 2006.

ESURFD
3, 1509–1553, 2015

Church, M. and Hassan, M. A.: Size and distance of travel of unconstrained clasts on a streambed, Water Resour. Res., 28, 299–303, doi:10.1029/91WR02523, 1992.
Constantinescu, G., Miyawaki, S., Rhoads, B. L., and Sukhodolov, A.: Numerical analysis of the effect of momentum ratio on the dynamics and sediment-entrainment capacity of coherent flow structures at a stream confluence, J. Geophys. Res., 117, F04028, doi:10.1029/2012JF002452, 2012.
Ferguson, R. and Wathen, S.: Tracer-pebble movement along a concave river profile?: Virtual velocity in relation to grain size and shear stress transport and deposition, Water Resour. Res., 34, 2031–2038, 1998.
Ferguson, R., Cudden, J. R., Hoey, T. B., and Rice, S. P.: River system discontinuities due to lateral inputs: generic styles and controls, Earth Surf. Proc. Land., 31, 1149–1166, doi:10.1002/esp.1309, 2006.
Fryirs, K.: (Dis)Connectivity in catchment sediment cascades: a fresh look at the sediment delivery problem, Earth Surf. Proc. Land., 38, 30–46, doi:10.1002/esp.3242, 2013.
Gayer, E., Mukhopadhyay, S., and Meade, B. J.: Spatial variability of erosion rates inferred from the frequency distribution of cosmogenic 3He in olivines from Hawaiian river sediments, Earth Planet. Sc. Lett., 266, 303–315, doi:10.1016/j.epsl.2007.11.019, 2008.
Gomi, T., Sidle, R. C., and Richardson, J. S.: Understanding processes and downstream linkages of headwater systems, Bioscience, 52, 905–916, doi:10.1641/0006-3568(2002)052[0905:UPADLO]2.0.CO;2, 2002.
Haschenburger, J. K.: Tracing river gravels: insights into dispersion from a long-term field experiment, Geomorphology, 200, 121–131, doi:10.1016/j.geomorph.2013.03.033, 2013.
Hassan, M. A., Church, M., and Schick, A. P.: Distance of movement of coarse particles in gravel bed streams, Water Resour. Res., 27, 503–511, 1991.
Hassan, M. A., Voepel, H., Schumer, R., Parker, G., and Fraccarollo, L.: Displacement characteristics of coarse fluvial bed sediment, J. Geophys. Res.-Earth, 118, 155–165, doi:10.1029/2012JF002374, 2013.
Hoffman, D. F. and Gabet, E. J.: Effects of sediment pulses on channel morphology in a gravel-bed river, Geol. Soc. Am. Bull., 119, 116–125, doi:10.1130/B25982.1, 2007.
Hubbell, D. and Sayre, W.: Sand transport studies with radioactive tracers, J. Hydraul. Div., 90, 39–68, 1964.
Imhoff, K. I.: Sediment Routing Through Channel Confluences: Particle Tracing in a Gravel-Bed River Headwaters, MS thesis, University of Montana, Missoula, MT, 2015.

ESURFD
3, 1509–1553, 2015

Coarse bedload routing and dispersion through tributary confluences

K. S. Imhoff and A. C. Wilcox

Kasprak, A., Wheaton, J. M., Ashmore, P. E., Hensleigh, J. W., and Peirce, S.: The relationship between particle travel distance and channel morphology?: Results from physical models of braided rivers, J. Geophys. Res. Earth Surf., 120, 55–74, doi:10.1002/2014JF003310, 2014.
Knighton, A. D.: Longitudinal changes in size and sorting of stream-bed material in four English rivers, Geol. Soc. Am. Bull., 91, 55–62, 1980.
Lajeunesse, E., Malverti, L., and Charru, F.: Bed load transport in turbulent flow at the grain scale: experiments and modeling, J. Geophys. Res., 115, F04001, doi:10.1029/2009JF001628, 2010.
Lamarre, H. and Roy, A. G.: The role of morphology on the displacement of particles in a step–pool river system, Geomorphology, 99, 270–279, doi:10.1016/j.geomorph.2007.11.005, 2008.
Lamarre, H., MacVicar, B., and Roy, A. G.: Using passive integrated transponder (PIT) tags to investigate sediment transport in gravel-bed rivers, J. Sediment. Res., 75, 736–741, doi:10.2110/jsr.2005.059, 2005.
Lancaster, S. T. and Casebeer, N. E.: Sediment storage and evacuation in headwater valleys at the transition between debris-flow and fluvial processes, Geology, 35, 1027–1030, doi:10.1130/G239365A.1, 2007.
Liébault, F., Bellot, H., Chapuis, M., Klotz, S., and Deschâtres, M.: Bedload tracing in a high-sediment-load mountain stream, Earth Surf. Proc. Land., 37, 385–399, doi:10.1002/esp.2245, 2012.
Lisle, T. E., Cui, Y., Parker, G., Pizzuto, J. E., and Dodd, A. M.: The dominance of dispersion in the evolution of bed material waves in gravel-bed rivers, Earth Surf. Proc. Land., 26, 1409–1420, doi:10.1002/esp.300, 2001.
Malmon, D. V., Reneau, S. L., Dunne, T., Katzman, D., and Drakos, P. G.: Influence of sediment storage on downstream delivery of contaminated sediment, Water Resour. Res., 41, 1–17, doi:10.1029/2004WR003288, 2005.
Martin, R. L., Jerolmack, D. J., and Schumer, R.: The physical basis for anomalous diffusion in bed load transport, J. Geophys. Res., 117, F01018, doi:10.1029/2011JF002075, 2012.
Milan, D. J.: Sediment routing hypothesis for pool-riffle maintenance, Earth Surf. Proc. Land., 38, 1623–1641, doi:10.1002/esp.3395, 2013.
Montgomery, D. R and Buffington, J. M.: Channel-reach morphology in mountain drainage basins, Geol. Soc. Am. Bull., 109, 596–611, 1997.
Mosley, M. P.: An experimental study of channel confluences, J. Geol., 84, 535–562, 1976.

ESURFD
3, 1509–1553, 2015

Mueller, E. R., Pitlick, J., and Nelson, J. M.: Variation in the reference Shields stress for bed load transport in gravel-bed streams and rivers, Water Resour. Res., 41, F02016, doi:10.1029/2004WR003692, 2005.

Olinde, L. and Johnson, J. P. L.: Using RFID and accelerometer-embedded tracers to measure probabilities of bed load transport, step lengths, and rest times in a mountain stream, Water Resour. Res., 51, 7572–7589, doi:10.1002/2014WR016120, 2015.

Parrett, C., Cannon, S., and Pierce, K.: Wildfire-Related Floods and Debris Flows in Montana in 2000 and 2001, USGS Water-Resources Investigations Rep. 03–4319, Reston, VA, 2004.

Phillips, C. B. and Jerolmack, D. J.: Dynamics and mechanics of bed-load tracer particles, Earth Surf. Dynam., 2, 513–530, doi:10.5194/esurf-2-513-2014, 2014.

Phillips, C. B., Martin, R. L., and Jerolmack, D. J.: Impulse framework for unsteady flows reveals superdiffusive bed load transport, Geophys. Res. Lett., 40, 1328–1333, doi:10.1002/grl.50323, 2013.

Prosser, I. P., Rutherfurd, I. D., Olley, J. M., Young, W. J., Wallbrink, P. J., and Moran, C. J.: Large-scale patterns of erosion and sediment transport in river networks, with examples from Australia, Mar. Freshwater Res., 52, 81–99, doi:10.1071/MF00033_CO, 2001.

Pyrce, R. S. and Ashmore, P. E.: The relation between particle step length distributions and channel morphology in gravel-bed streams: a synthesis, Geomorphology, 56, 167–187, doi:10.1016/S0169-555X(03)00077-1, 2003.

Recking, A.: Simple method for calculating reach-averaged bed-load transport, J. Hydraul. Eng.-ASCE, 139, 70–75, doi:10.1061/(ASCE)HY.1943-7900.0000653, 2013.

Rhoads, B. L.: Changes in stream channel characteristics at tributary junctions, Phys. Geogr., 8, 346–361, doi:10.1080/02723646.1987.10642333, 1987.

Rhoads, B. L. and Sukhodolov, A. N.: Spatial and temporal structure of shear layer turbulence at a stream confluence, Water Resour. Res., 40, W06304, doi:10.1029/2003WR002811, 2004.

Rhoads, B. L., Riley, J. D., and Mayer, D. R.: Response of bed morphology and bed material texture to hydrological conditions at an asymmetrical stream confluence, Geomorphology, 109, 161–173, doi:10.1016/j.geomorph.2009.02.029, 2009.

Ribeiro, M. L., Blanckaert, K., Roy, A. G., and Schleiss, A. J.: Flow and sediment dynamics in channel confluences, J. Geophys. Res., 117, F01035, doi:10.1029/2011JF002171, 2012.

Rice, S. P., Greenwood, M. T., and Joyce, C. B.: Tributaries, sediment sources, and the longitudinal organisation of macroinvertebrate fauna along river systems, Can. J. Fish. Aquat. Sci., 58, 824–840, doi:10.1139/cjfas-58-4-824, 2001.

ESURFD
3, 1509–1553, 2015

Richards, K. S.: A note on changes in channel geometry at tributary junctions, Water Resour. Res., 16, 241–244, doi:10.1029/WR016i001p00241, 1980.

Roy, A. G. and Bergeron, N.: Flow and particle paths at a natural river confluence with coarse bed material, Geomorphology, 3, 99–112, doi:10.1016/0169-555X(90)90039-S, 1990.

Sklar, L. S., Fadde, J., Venditti, J. G., Nelson, P., Wydzga, M. A., Cui, Y., and Dietrich, W. E.: Translation and dispersion of sediment pulses in flume experiments simulating gravel augmentation below dams, Water Resour. Res., 45, W08439, doi:10.1029/2008WR007346, 2009.

Strahler, A. N.: Hypsometric (area-altitude) analysis of erosional topography, Geol. Soc. Am. Bull., 63, 1117–1142, doi:10.1130/0016-7606(1952)63[1117:HAAOET]2.0.CO;2, 1952.

Swanson, F. J. and Fredriksen, R. L.: Sediment routing and budgets?: Implications for judging impacts of forestry practices, in: Sediment Budgets and Routing in Forested Drainage Basins, edited by: Swanson, F. J., Janda, R. J., Dunne, T., and Swanston, D. N., U.S. Forest Service, Portland, OR, 129–137, 1982.

Swanson, B. J. and Meyer, G.: Tributary confluences and discontinuities in channel form and sediment texture: Rio Chama, NM, Earth Surf. Proc. Land., 39, 1927–1943, doi:10.1002/esp.3586, 2014.

Tooth, S., McCarthy, T. S., Brandt, D., Hancox, P. J., and Morris, R.: Geological controls on the formation of alluvial meanders and floodplain wetlands: the example of the Klip River, eastern Free State, South Africa, Earth Surf. Proc. Land., 27, 797–815, doi:10.1002/esp.353, 2002.

Yang, C. and Sayre, W.: Stochastic model for sand dispersion, J. Hydraul. Div., 97, 265–288, 1971.

ESURFD
3, 1509–1553, 2015

Table 1. Geometric and grain-size characteristics of the bed at each study reach. Width and depth values are at bankfull along the cross-sections taken at each location. Upper and lower confluences reaches are denoted with (U) and (L), respectively.

Study Reach	S	Width (m)	Depth (m)	D_{50} (m)	D_{84} (m)	Q_r (avg)	θ	z_d (m)
Moose Creek (U)	0.018	11	0.76	0.05	0.10	0.63	86°	0.16
Martin Creek (U)	0.029	7	0.94	0.06	0.15			
Control Reach	0.016	15	0.78	0.06	0.13	–	–	–
Martin Creek (L)	0.017	15	0.80	0.07	0.12	0.45	81°	0
East Fk. Bitterroot (L)	0.016	16	1.03	0.07	0.14			

ESURFD
3, 1509–1553, 2015

Table 2. Tracer recovery and transport statistics by study reach.

Study Reach	n^{a}	$n_{rec}{}^{b}$	Recovery (%)	D_{50} (m)	$(X^{c} \pm \sigma^{d})_{tot}$ (m)	$(X \pm \sigma)_{mob}$ (m)	X_{max} (m)
Moose Creek (U)	65	53	82	0.077	7.4 ± 6.6	8.5 ± 6.4	24.5
Martin Creek (U)	62	42	68	0.081	3.8 ± 4.1	4.4 ± 4.1	20.6
Control Reach	97	83	86	0.080	4.2 ± 5.3	4.9 ± 5.4	22.7
Martin Creek (L)	103	71	68	0.082	14.6 ± 22.9	16.4 ± 24	133
East Fk. Bitterroot (L)	101	74	73	0.080	47.4 ± 56.3	49.4 ± 56.6	211

[a] number of tracers deployed.
[b] number of tracers recovered.
[c] average transport distance.
[d] standard deviation.
"tot" and "mob" describe (1) the total tracer population and (2) tracers moving beyond 0.5 m.

ESURFD
3, 1509–1553, 2015

Table 3. Model-derived tracer statistics.

Study Reach	EHS (Mueller) X	σ	CV*	GEM (Mueller) X	σ	CV
Moose Creek (U)	6.7	5.7	0.86	6.6	5.7	0.87
Martin Creek (U)	3.8	3.8	1.0	3.8	3.9	1.0
Control Reach	4.2	4.6	1.1	4.2	4.6	1.1
Martin Creek (L)	15.6	24.6	1.6	16.2	25.1	1.6
East Fk. Bitterroot (L)	43.9	61.4	1.4	43.7	61.0	1.4
Study Reach	EHS (Recking) X	σ	CV	GEM (Recking) X	σ	CV
Moose Creek (U)	6.8	5.8	0.86	6.8	5.8	0.86
Martin Creek (U)	3.8	3.8	1.0	3.8	3.9	1.0
Control Reach	4.2	4.6	1.1	4.3	4.8	1.1
Martin Creek (L)	15.7	24.7	1.6	16.1	25.1	1.6
East Fk. Bitterroot (L)	44.0	61.5	1.4	43.6	61.0	1.4

* coefficient of variation.

ESURFD
3, 1509–1553, 2015

Table 4. Critical shear velocity (U_c*) and dimensionless impulse (I^*) at each study reach.

Study Reach	τ^*_c	$\tau^*_{c,\text{Mueller}}$ U^*_c ($m\,s^{-1}$)	I^*	τ^*_c	$\tau^*_{c,\text{Recking}}$ U^*_c ($m\,s^{-1}$)	I^*
Moose Creek (U)	0.06	0.23	602 000	0.08	0.27	14 900
Martin Creek (U)	0.08	0.29	310 000	0.11	0.34	37 600
Control Reach	0.06	0.23	425 000	0.07	0.25	88 400
Martin Creek (L)	0.06	0.25	1 200 000	0.09	0.31	86 000
East Fk. Bitterroot (L)	0.06	0.25	1 900 000	0.07	0.29	577 000

ESURFD
3, 1509–1553, 2015

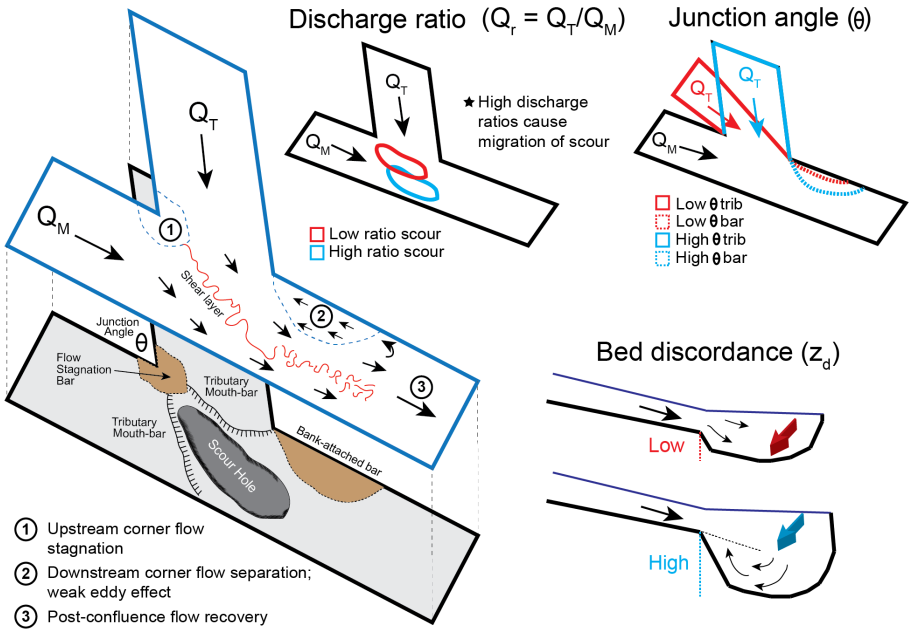

Figure 1. Flow (top left) and morphology (bottom left) in a gravel-bed confluence (after Best, 1987). Key variables influencing hydraulics and morphology include discharge ratio (Q_r), junction angle (θ), bed discordance (z_d), and upstream planform geometry (not pictured).

ESURFD
3, 1509–1553, 2015

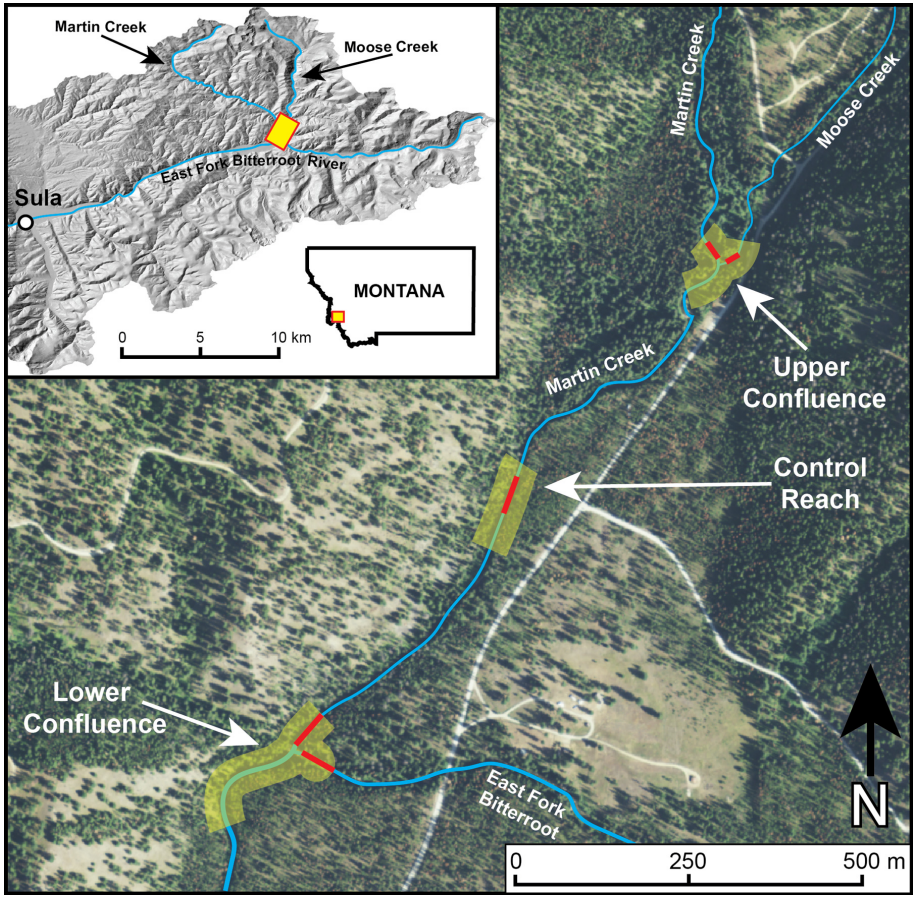

Figure 2. Study area, including location within the East Fork Bitterroot River's headwaters (upper left) and three study sites: upper and lower confluences and a control reach, outlined in yellow; individual reaches in which PIT-tagged particles were seeded are outlined in red.

ESURFD
3, 1509–1553, 2015

Coarse bedload routing and dispersion through tributary confluences

K. S. Imhoff and
A. C. Wilcox

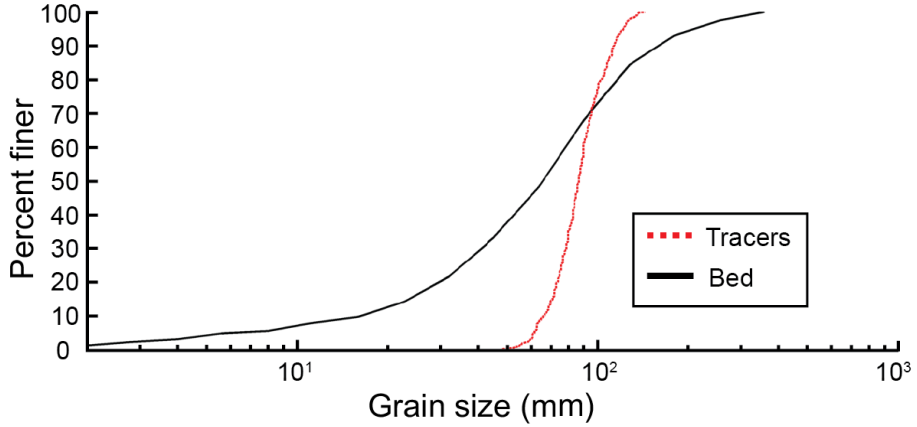

Figure 3. (a) Grain size distribution of tagged tracers (red) as compared to the streambed (black) composite over all study sites. Below are photographs of the **(b)** upper confluence, **(c)** control reach, and **(d)** lower confluence.

ESURFD
3, 1509–1553, 2015

Coarse bedload routing and dispersion through tributary confluences

K. S. Imhoff and
A. C. Wilcox

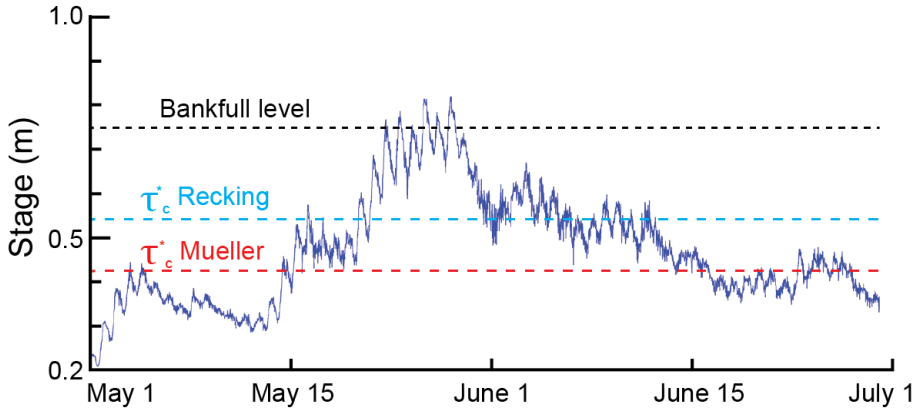

Figure 4. Stage hydrograph during spring 2014 runoff period at lower confluence (East Fork Bitterroot River) study site. Estimated bankfull level, based on cross-section topography surveyed at transducer location, is shown as horizontal dotted line.

ESURFD
3, 1509–1553, 2015

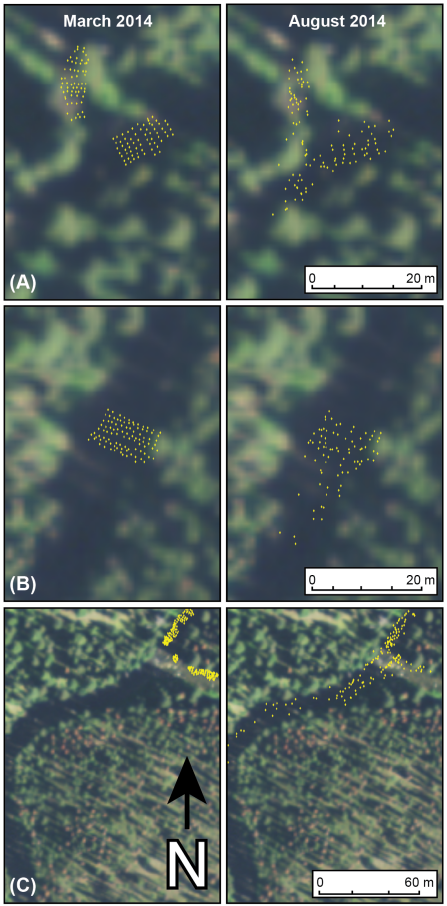

Figure 5. Tracer positions at initial installation (left) and following the 2014 flood (right).

ESURFD
3, 1509–1553, 2015

Coarse bedload routing and dispersion through tributary confluences

K. S. Imhoff and
A. C. Wilcox

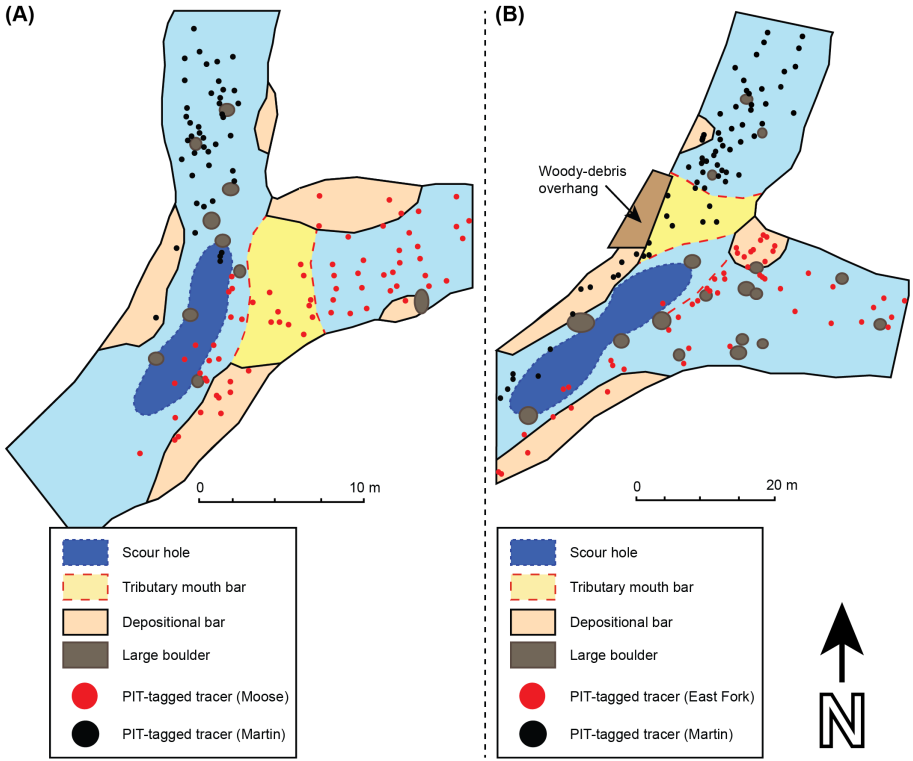

Figure 6. Digitized patch map of bedforms and tracer recovery positions at the **(a)** upper and **(b)** lower confluences.

ESURFD
3, 1509–1553, 2015

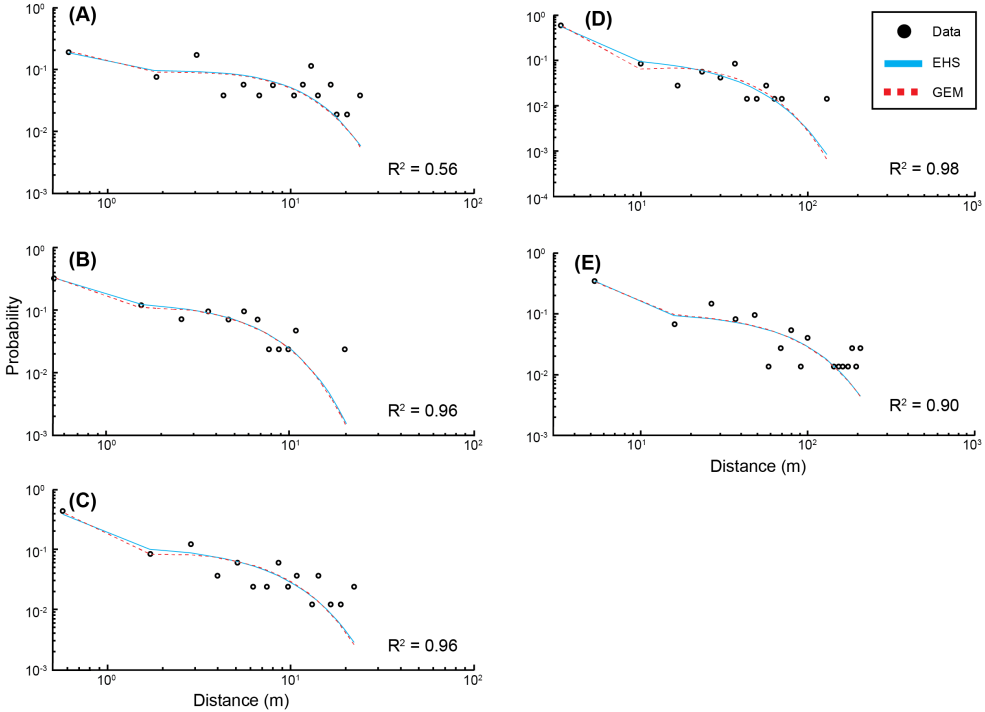

Figure 7. Einstein–Hubbell–Sayre (EHS) and Yang–Sayre (GEM) model fits for **(a)** Moose Creek, **(b)** Martin Creek (upper), **(c)** the control reach, **(d)** Martin Creek (lower), and **(e)** the East Fork Bitterroot River. R^2 fit differences between the two models were < 0.01, so we present their shared fit values here.

ESURFD
3, 1509–1553, 2015

Coarse bedload routing and dispersion through tributary confluences

K. S. Imhoff and
A. C. Wilcox

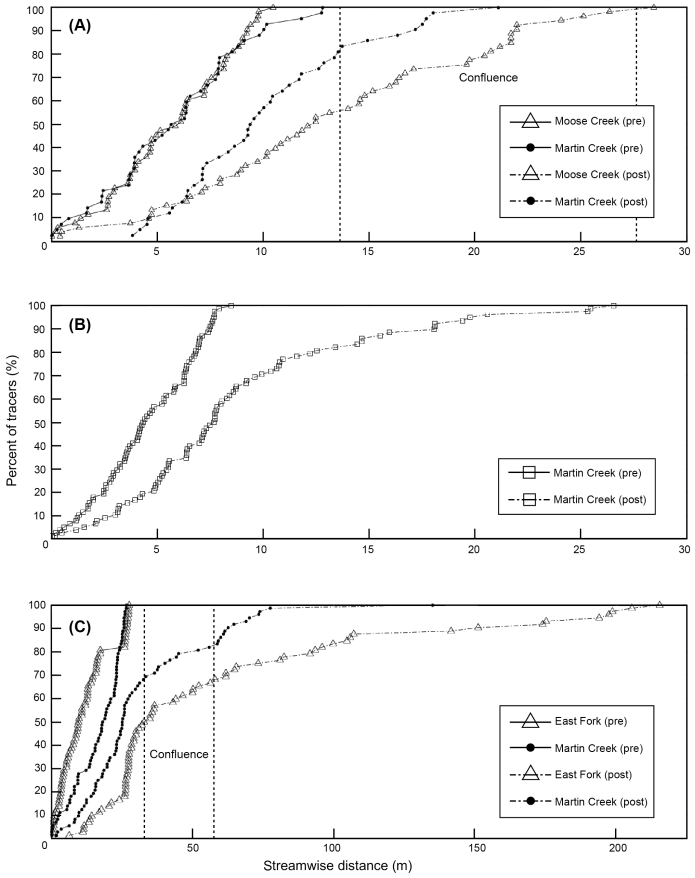

Figure 8. Spatial distribution of tracer positions at the time of initial deployment (pre) and after the 2014 flood (post) for **(a)** the upper confluence, **(b)** the control reach, and **(c)** the lower confluence. The confluence zones are bracketed with dotted vertical lines. Note the altered *x* axis scale in **(c)**.

ESURFD
3, 1509–1553, 2015

Coarse bedload routing and dispersion through tributary confluences

K. S. Imhoff and
A. C. Wilcox

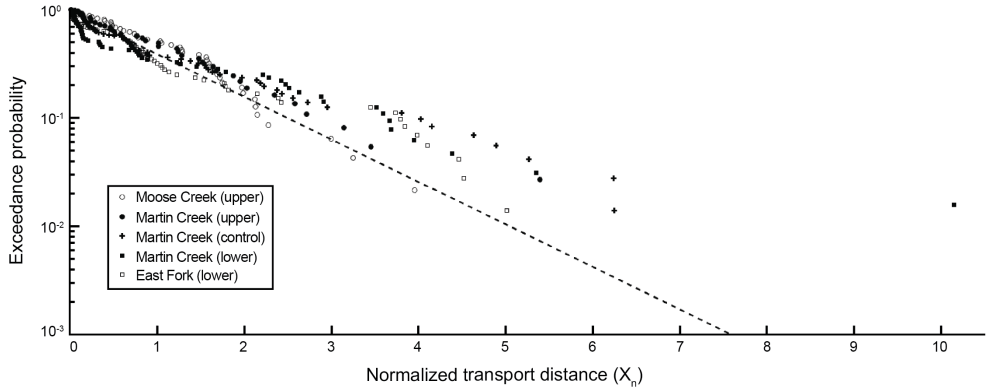

Figure 9. Normalized transport distances (X_n) in all five study reaches (Eq. 1).

ESURFD
3, 1509–1553, 2015

Coarse bedload routing and dispersion through tributary confluences

K. S. Imhoff and
A. C. Wilcox

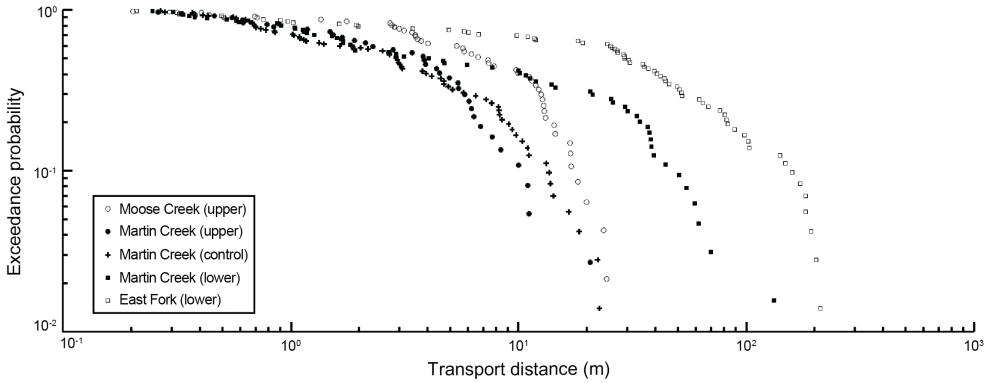

Figure 10. Cumulative exceedance distributions of travel distance for the upper confluence, lower confluence, and control reach.

ESURFD
3, 1509–1553, 2015

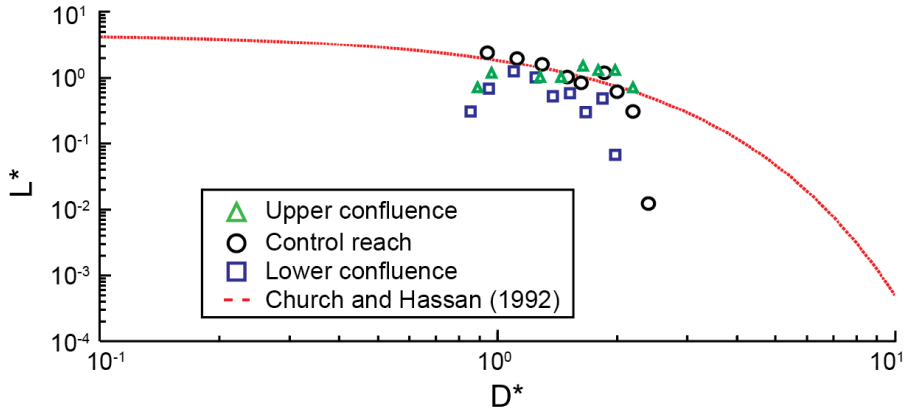

Figure 11. Church and Hassan's (1992) relationship (Eq. 2) between scaled travel distance (L^*) and scaled particle size (D^*) during the 2014 hydrograph. L^* and D^* are scaled by median L and D values for each tracer sub-population. Both study confluences are combined into a single population.

ESURFD
3, 1509–1553, 2015

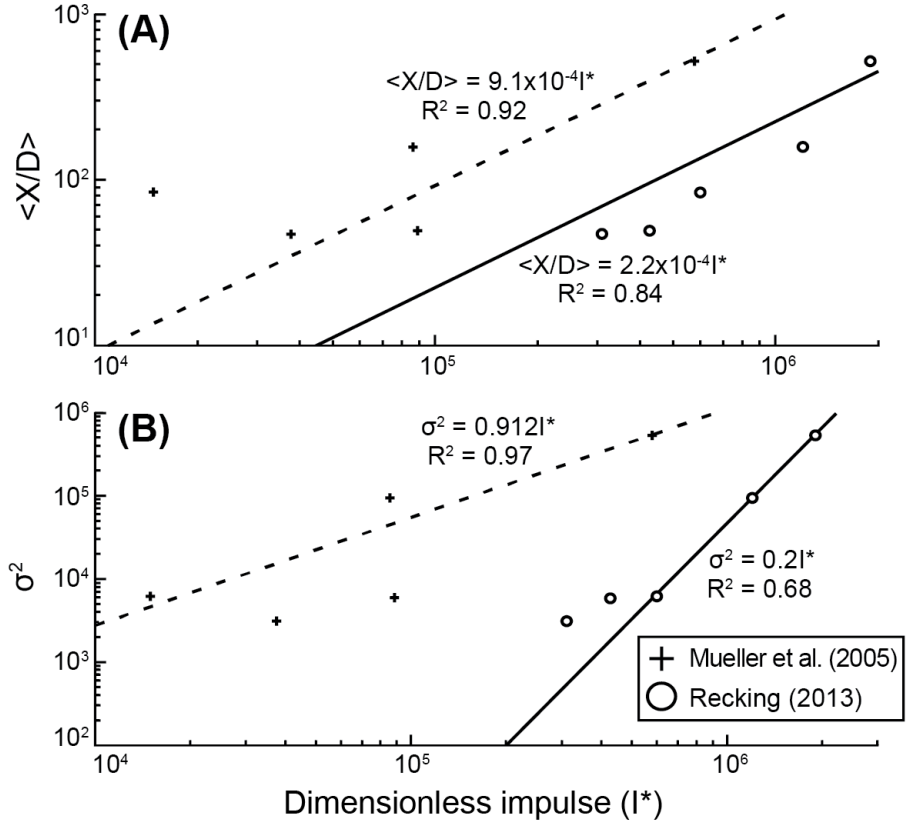

Figure 12. Linear and power-law relations between dimensionless impulse (I^*) and **(a)** $\langle X/D \rangle$ and **(b)** σ^2.

ESURFD
3, 1509–1553, 2015

Coarse bedload routing and dispersion through tributary confluences

K. S. Imhoff and
A. C. Wilcox

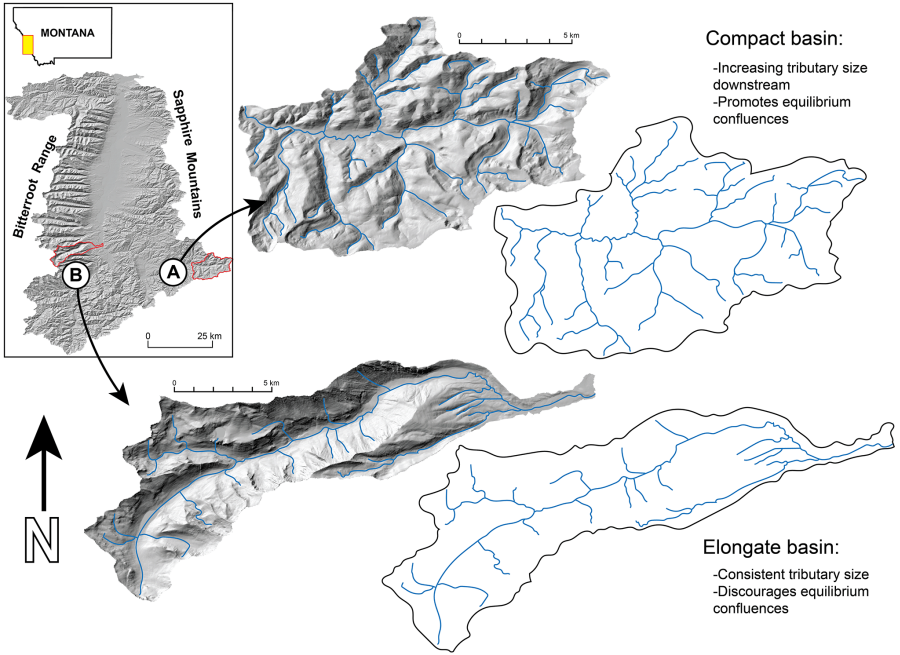

Figure 13. Typical basin shapes and tributary sizes in the (A) Sapphire Mountains (East Fork Bitterroot River) and (B) Bitterroot Range (Tin Cup Creek). These basins are of similar drainage area, but differ in lithology, erosional history, basin morphology, and potential sediment routing.

ESURFD
3, 1509–1553, 2015